Journal of Materials Chemistry B

PAPER

View Article Online
View Journal

Cite this: DOI: 10.1039/c7tb02609a

A simple mitochondrial targeting AIEgen for image-guided two-photon excited photodynamic therapy†

Meijuan Jiang,[ab] Ryan T. K. Kwok,[ab] Xuesong Li,[c] Chen Gui,[ab] Jacky W. Y. Lam,[ab] Jianan Qu[c] and Ben Zhong Tang*[abd]

Received 29th September 2017,
Accepted 30th October 2017

DOI: 10.1039/c7tb02609a

rsc.li/materials-b

Two-photon excited photodynamic therapy (TP-PDT) is not only able to offer deeper penetration depth but also much more precise 3D treatment than traditional one-photon excited PDT. However, the achievement of TP-PDT requires photosensitizers with large two-photon absorption cross sections, efficient generation of reactive oxygen species, and bright two-photon fluorescence. In this work, we present a simple AIE luminogen (AIEgen), IQ-TPA, with mitochondrial targeting and susceptible two-photon excitation for image-guided photodynamic therapy in cancer cells. This feasibility of utilizing small molecular multifunctional AIEgens for TP-PDT was demonstrated together with the merits of tiny size, good cell permeability, low dark cytotoxicity and easy synthesis, showing great potential for the development of future theranostic systems.

Introduction

Cancer is the leading cause of death worldwide, thus its diagnosis and treatment have received enormous attention in life science and clinical research. Photodynamic therapy (PDT), which relies on the reactive oxygen species (ROS) generated by photosensitizers (PSs) upon light irradiation to kill diseased cells, is gaining clinical use due to it being less invasive, its lower toxicity, and its higher spatial resolution in eliminating malignant tumor cells as compared to chemotherapy.[1] The most widely used PDT photosensitizers are porphyrin and phenothiazinium derivatives.[2] However, these traditional PSs suffer from some limitations: (1) aggregation-caused quenching (ACQ) in fluorescence and reduced PDT efficiency due to hydrophobic and rigid planar structures;[3] (2) poor cell permeability, for which long incubation times, high dye concentrations and tedious modifications are required to achieve effective PDT; (3) short-wavelength excitation, which leads to low penetration depth and thus they are only capable of treating cancers of the skin and hollow organs. The full potential of PDT has not yet been achieved. Therefore, it is highly in demand to develop PSs that can address these problems.

To address the ACQ problem, dilute solutions of PSs or nanocarriers with a low loading of PSs were used. However, this generates another problem: such a small number of molecules are easily photobleached under laser irradiation, losing both the imaging and PDT functions. The combination of imaging and PDT, namely image-guided PDT, is of significance to fundamental and clinical research as it enables the detection of targets, tracking of drug distribution and evaluation of the therapeutic effect simultaneously in one system. Alternatively, materials with aggregation-induced emission (AIE) characteristics offer a good solution. In contrast to ACQ luminogens, AIE luminogens (AIEgens) generally have rotor–stator structures and exhibit weak emission in good solvents, but they become highly emissive in the aggregated state due to the restriction of intramolecular motion (RIM).[4] The exploration of AIEgens in biological applications has enjoyed great successes, such as in the intracellular sensing of chemicals[5] or biological analytes,[6] localization of organelles,[7] tracking of cells,[8] and imaging of tumors[9] with the merits of a large Stokes shift, high brightness

[a] Department of Chemistry, Hong Kong Branch of Chinese National Engineering Research Centre for Tissue Restoration and Reconstruction, Institute for Advanced Study, Institute of Molecular Functional Materials, State Key Laboratory of Molecular Neuroscience, Division of Life Science, Hong Kong University of Science and Technology, Clear Water Bay, Kowloon, Hong Kong. E-mail: tangbenz@ust.hk
[b] Guangdong Provincial Key Laboratory of Brain Science, Disease and Drug Development, HKUST-Shenzhen Research Institute, No. 9 Yuexing 1st RD, South Area, Hi-tech Park, Nanshan, Shenzhen 518057, China
[c] Department of Electronic and Computer Engineering, Center of Systems Biology and Human Health, School of Science and Institute for Advanced Study, Hong Kong University of Science and Technology, Clear Water Bay, Kowloon, Hong Kong, China
[d] Guangdong Innovative Research Team, SCUT-HKUST Joint Research Laboratory, State Key Laboratory of Luminescent Materials and Devices, South China University of Technology, Guangzhou 510640, China

† Electronic supplementary information (ESI) available: Experimental section, NMR, mass, supplementary photophysical properties, cell viability and cell imaging. See DOI: 10.1039/c7tb02609a

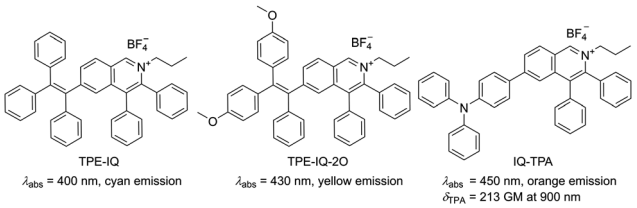

Chart 1 Chemical structures of mitochondrial targeting AIE PSs, their absorption maxima and emission colours in cell imaging and the two-photon absorption cross section (δ_{TPA}) of IQ-TPA are given.

and good photostability.[4,10] Unlike the fluorescence quenching and reduced PDT efficacy of traditional PSs, AIE PSs show enhanced fluorescence and efficient phototoxicity in the aggregated state,[11] making them promising for application in fluorescence image-guided PDT.

To maximize the efficacy of PDT, intracellular targetability is crucial in the rational design of PSs due to the high reactivity and short half-life of the ROS. Among numerous targeting organelles, mitochondria are of significance to improve the PDT effect due to their vital role as the power station and contribution in maintaining normal physiological activity.[12] So far, several AIE PSs with mitochondrial specificity have been developed, such as TPE-IQ and TPE-IQ-2O (Chart 1).[12d,13] They can fast permeate cells and induce cell apoptosis effectively at low concentrations under light irradiation. More interestingly, it is known that most cancer cells have a higher mitochondrial membrane potential (MMP) than most normal cells[14] and thus the cationic dyes can preferentially accumulate and be retained in cancer cells. Subsequently, these mitochondrial targeting AIE PSs could be further utilized for selective light-up and killing of cancer cells (Scheme 1).[12c,13a] So far, the AIE PSs developed have a problem of short excitation wavelengths in the UV or visible region due to the poor conjugation of rotor structures. Synthetically, to access PSs with one-photon NIR excitation is of great difficulty due to the fact that (1) it requires an effective intersystem crossing (ISC) and a higher energy level of the triplet state of the PS than that of the singlet state of the oxygen molecule; (2) an extension of π conjugation is needed but it will bring about the intrinsic disadvantages of increasing molecular weight, poor water solubility and synthetic complexity; and (3) one-photon excitation cannot go beyond 750 nm as there is insufficient energy for singlet oxygen production.[15] Therefore, two-photon excitation, using two NIR photons instead of a single visible photon, has been widely promoted in PDT.[16] PSs with two-photon excitation are applicable in treatments not only for superficial diseases but also for solid tumors with deep penetration depth. More importantly, a better *z*-axial resolution can be achieved without damaging healthy cells in the light beam path due to the nonlinear optical phenomenon (Scheme 2). Such a high 3D spatial selectivity of two-photon excited PDT (TP-PDT) has been demonstrated by the selective closure of tiny blood vessels *in vivo*[16b,17] and is crucial for the delicate treatment of eye or brain-related diseases, such as the wet-form of aged-related macular degeneration, an eye disease that will cause blindness in the older population.[18] Therefore, to develop

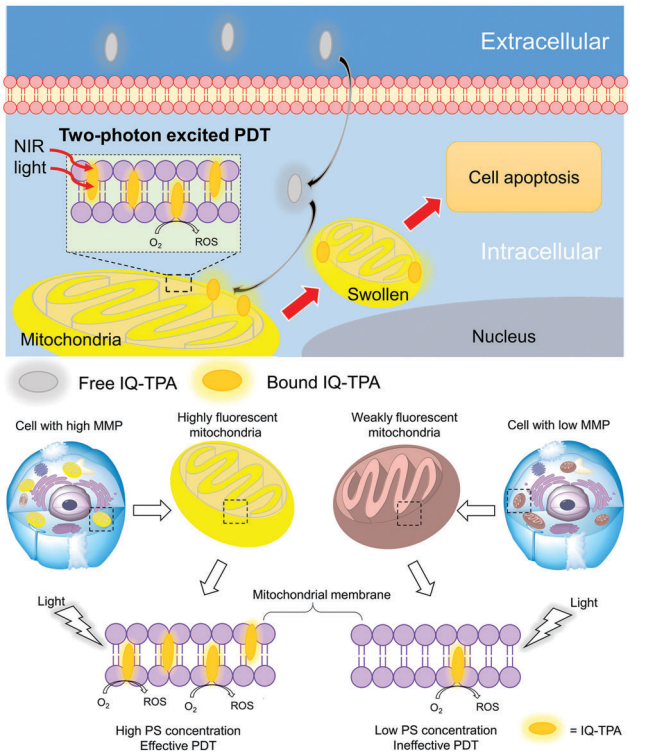

Scheme 1 Application of mitochondrial targeting AIEgen (IQ-TPA) for image-guided two-photon excited photodynamic therapy (TP-PDT) *via* ROS-induced cell apoptosis and to selectively kill cells with high mitochondrial membrane potential (MMP). ROS: reactive oxygen species.

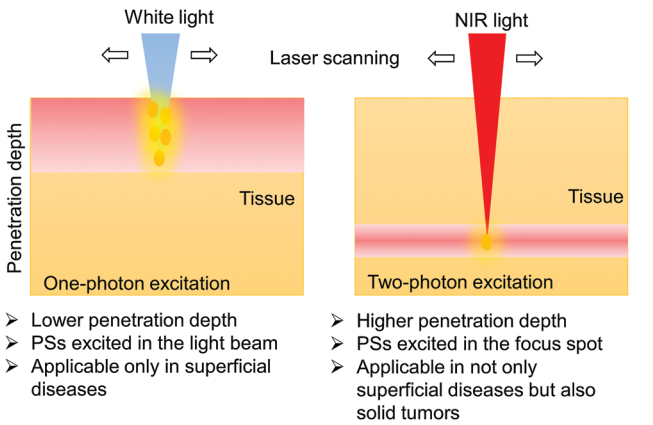

Scheme 2 Comparison of one-photon excitation and two-photon excitation in photodynamic therapy.

AIE PSs with susceptible two-photon excitation is significant for precise cancer treatment.

To improve the low two-photon absorption (TPA) cross section (δ_{TPA}), useful efforts have been made in constructing energy-transferring cassettes using dyes with large δ_{TPA} as energy donors encapsulated in nanoparticles.[15c,19] However, this approach encounters drawbacks, including the difficult control of energy transfer efficacy, a large size-induced transport barrier and complex fabrication with poor reproducibility.[20] Instead, directly improving the intrinsic δ_{TPA} of existing small molecular

PSs will enjoy the merits of tiny size, good cell permeability, minimal perturbation to living systems and easy synthesis.[15b] This one-for-all approach will greatly simplify the fabrication process and improve reproducibility, benefiting practical applications. Herein, a triphenylamine group was introduced to replace the TPE structure of TPE-IQ to obtain a mitochondrial targeting AIE PS, namely IQ-TPA (Chart 1). Indeed, the resulting compound IQ-TPA possessed a large δ_{TPA} of 213 GM, efficient ROS generation and mitochondrial targeting property and its feasibility for image-guided TP-PDT in cancer cell ablation was also demonstrated *in vitro*.

Experimental section

Materials and instruments

Pentamethylcyclopentadienylrhodium(III) chloride dimer ($[RhCp^*Cl_2]_2$), and silver boron fluoride ($AgBF_4$) were purchased from J&K Scientific. Mitotracker Red FM, Mitotracker Green FM, minimum essential medium (MEM), fetal bovine serum (FBS), penicillin and streptomycin were purchased from Invitrogen. Propidium iodide (PI), fluorescein diacetate (FDA), 2′,7′-dichlorodihydrofluorescein diacetate (DCFH-DA), 3-(4,5-dimethylthiazol-2-yl)-2,5-diphenyltetrazolium bromide (MTT) and other chemicals were all purchased from Sigma-Aldrich and used as received without further purification. Milli-Q water was supplied by Milli-Q Plus System (Millipore Corporation, Breford, USA). ^1H and ^{13}C NMR spectra were measured on a Bruker ARX 400 NMR spectrometer using DMSO-d_6 and $CDCl_3$ as solvents and tetramethylsilane (TMS) as internal reference. High-resolution mass spectra (HR-MS) were recorded on a Finnigan MAT TSQ 7000 Mass Spectrometer System operating in a MALDI-TOF mode. UV absorption spectra were taken on a Milton Ray Spectronic 3000 array spectrophotometer. Photoluminescence (PL) spectra were recorded on a Perkin-Elmer spectrofluorometer LS 55.

Synthesis

For synthetic procedures of IQ-TPA, please refer to a previous report.[21] ^1H NMR (400 MHz, DMSO-d_6) δ (ppm) 10.29 (s, 1H), 8.66 (d, 1H, J = 8.8 Hz), 8.43(d, 1H, J = 8.4 Hz), 7.60–7.58 (m, 3H), 7.49 (s, 2H), 7.40–7.28 (m, 12H), 7.15–7.08 (m, 6H), 7.00 (d, 2H, J = 8.4 Hz), 4.36 (t, 2H, J = 7.2 Hz), 1.85–1.80 (m, 2H), 0.79 (t, 3H, J = 7.2 Hz). ^{13}C NMR (100 MHz, DMSO-d_6) δ (ppm) 149.3, 149.1, 147.7, 146.3, 144.3, 137.9, 137.7, 133.5, 131.4, 131.1, 130.4, 130.3, 130.1, 130.0, 129.8, 128.7, 128.5, 128.3, 125.5, 125.2, 124.3, 121.6, 120.8, 60.0, 23.7, 10.5 ppm. ^{19}F NMR (376 MHz, DMSO-d_6) δ (ppm) −148.3. MS (MALDI-TOF): calculated for cation of IQ-TPA ($C_{42}H_{35}N_2^+$): 567.2795, found: 567.2771.

Cell culture

HeLa cells were cultured in MEM containing 10% FBS and antibiotics (100 units per mL penicillin and 100 g mL^{-1} streptomycin) in a 5% CO_2 humidity incubator at 37 °C and sub-cultured every 2 or 3 days.

Cell imaging

HeLa cells were grown overnight in a 35 mm Petri dish with a cover slip or a glass-bottom dish. The cell staining was conducted by replacing the cell medium with dye-containing medium. The cover slip with cells was mounted onto an iron slide with an observation window and imaged under an FL microscope (BX41 upright Microscope) using different combinations of excitation and emission filters for each dye. The glass-bottom dish with cells was observed on an inverted microscope directly.

Factors affecting photodynamic therapy evaluated by MTT assay

The HeLa cells were seeded in 24-well plates at a density of 30 000 cells per well with 1 mL of medium. After incubation for 24 h, the medium was replaced by 1 mL of medium with/without dye and the cells were subjected to light irradiation, followed by incubation at 37 °C for 24 h. Then 50 μL of MTT (0.5 mg mL^{-1}) solution in PBS was added into each well and the plate was kept at 37 °C in a cell incubator for 4 h. After gentle removal of the MTT containing medium, the formazan crystals were dissolved in 1 mL of DMSO with agitation. Then 100 μL of the solution was transferred into a 96 well plate for measurement. The absorbance was measured at 570 nm and 700 nm (background) using a microplate reader. After subtracting the background, the untreated cells served as the control and their viability was set to 100%. Each trial was performed with two wells parallel. Factors affecting PDT: (1) Influence of dye concentration. After incubation with IQ-TPA for 30 min at different concentrations in the incubator for 30 min, the cells were subjected to white LED light irradiation for 15 min at the power density of 60 mW cm^{-2}. (2) Influence of dye pre-incubation time before light irradiation. The cells were incubated with 1 μM IQ-TPA for 0, 15, 30, and 45 min followed by light irradiation for 15 min at the power of 60 mW cm^{-2}. (3) Influence of irradiation time. After incubation with IQ-TPA for 30 min at different concentrations in the incubator for 30 min, the cells were subjected to light irradiation for 0, 20 and 40 min at the power density of 60 mW cm^{-2}. (4) Influence of light density. After incubation with 1 μM IQ-TPA for 90 min, the cells were subjected to light irradiation of 0, 8, 22, 37, 57 and 60 mW cm^{-2} for 15 min.

ROS generation detection in cells

The HeLa cells were seeded in a 96-well plate at a density of 10 000 cells per well and incubated for 24 h. After being incubated with IQ-TPA at different concentrations for 0, 20, 40, and 60 min, the cells were washed with PBS and then incubated with 100 μL of 10 μM DCFH-DA in medium for 30 min. Then the cells were carefully washed with PBS twice and 100 μL of PBS was added. Then the plate was subjected to white LED light irradiation. The fluorescence signal was determined by a fluorescence plate reader at the time of 0, 5 and 10 min (excitation/emission: 488 nm/525 nm).

Monitoring mitochondrial morphology

HeLa cells were seeded on the cover slide in a 3.5 cm culture dish with 2 mL of medium. HeLa cells were pre-incubated with 1 μM IQ-TPA for 30 min and then observed under a fluorescent BX41 microscope (Olympus) using the excitation

light of 460–490 nm or with a cofocal laser microscope (Leica STED TCS SP5 II Confocal Laser Scanning Microscope) coupled with a femtosecond laser source (140 fs, 80 MHz).

PI staining of the cell death induced by PDT

HeLa cells were seeded on the cover slide in a 3.5 cm culture dish with 2 mL of medium. HeLa cells were pre-incubated with 1 μM IQ-TPA for 30 min and then subjected to white LED light irradiation for 15 min at the power of 60 mW cm^{-2}. A control group with dye staining and light irradiation alone was studied at the same time. After that, the cells were further incubated for 3 and 18 h. Then the cells were stained with 2 mL of 1.5 μM PI for 15 min in medium and observed under the fluorescence microscope.

Two-photon experiments

HeLa cells for the experiments were grown on glass-bottom dishes for 24 h. Prior to the intracellular ROS detection, HeLa cells were incubated with IQ-TPA (1 μM) and DCFH-DA (10 μM) for 30 min and washed with fresh medium twice. The cells were then subjected to different two-photon scans. The fluorescence images of DCF were captured at an interval of 20 scans. To assess the cell viability of TP-PDT, HeLa cells were incubated with IQ-TPA (1 μM, 30 min) and washed with fresh medium twice. The cells were then subjected to different two-photon scans at different laser powers. After 18 h post-incubation, the cells were stained with 2 μM FDA and 1.5 μM PI for 15 min and washed with fresh medium before imaging. The cell viability of the sample was estimated by the ratio of survival cell density of the scanned areas with that of the neighbouring unscanned area. The white light or laser power on the sample was estimated by an optical power meter (Newport, Model 1916-C).

Results and discussion

Synthesis and photophysical properties

The design principle of IQ-TPA was taken with the following considerations: (1) the intrinsic cationic structure was kept for mitochondrial targeting and it could serve as a strong electron acceptor; (2) triphenylamine is a popular building block for two-photon materials;[22] (3) triphenylamine could serve as a strong electron donor and the resulting large donor–π–acceptor (D–π–A) conjugation would be beneficial for two-photon absorption[23] and further red shift both the absorption/emission wavelengths; (4) the resulting multi-rotor structure was considered to render IQ-TPA with AIE characteristics. The synthesis of IQ-TPA can be simply achieved by following the previous procedures through a simple one-pot multicomponent reaction under the catalysis of a rhodium complex as shown in Scheme 3.[12d,21,24] The photophysical properties of IQ-TPA were then studied. As shown in Fig. 1A and B, IQ-TPA exhibits an absorption band peak at around 450 nm (ε: ~18 000 M^{-1} cm^{-1}) and ready two-photon excitation with a large δ_{TPA} of 215 GM at 900 nm. Compared to TPE-IQ-2O, the absorption maximum is red-shifted 20 nm and this should be attributed to the stronger

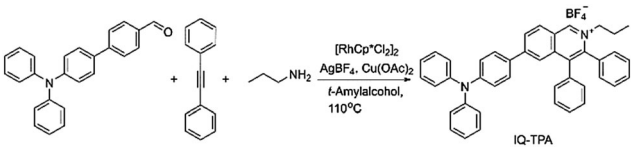

Scheme 3 Synthetic route of IQ-TPA.

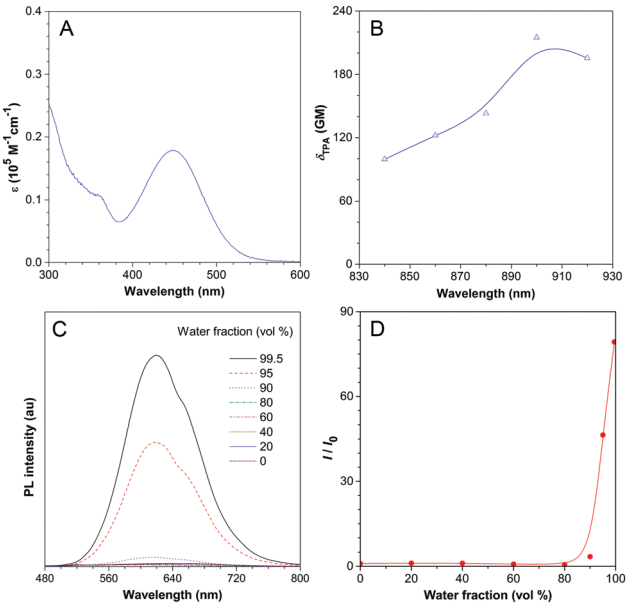

Fig. 1 (A) UV-vis absorption in DMSO and (B) two-photon absorption spectra of IQ-TPA. (C) Photoluminescence (PL) spectra of IQ-TPA in DMSO/water mixtures with various water fractions. (D) Plot of relative peak intensity of IQ-TPA in mixtures against water fraction. Dye concentration: 25 μM. Excitation: 450 nm.

electron-donating ability of triphenylamine. Considering the rather small molecular size of IQ-TPA (567.7 Da), the δ_{TPA} of IQ-TPA (215 GM) is much larger than those of the previously reported compounds for TP-PDT (10–50 GM),[18,25] demonstrating extension of the donor–π–acceptor (D–π–A) system and the attachment of the triphenylamine group can effectively increase the δ_{TPA}.[16d,26] To examine the AIE feature of IQ-TPA, its photoluminescence (PL) spectra were recorded in DMSO/water mixtures (Fig. 1C and D) by changing the composition of water in the mixtures. IQ-TPA emits weakly in mixtures with water fractions from 0 to 90 vol%. Due to its poor solubility in water, further increasing the water content led to aggregate formation and a strong emission peak at 622 nm was observed, exhibiting a typical AIE phenomenon. A large Stokes shift (172 nm) was found, which is beneficial for cell imaging to avoid the "inner-filter" effect.

ROS generation

During the PDT process, ROS plays a key role in killing the cells. Thus, we evaluated the ROS generation rate of IQ-TPA under white light irradiation using a commercial ROS indicator, namely DCFH, which is non-fluorescent and will be oxidized by ROS into a green fluorescent form, namely DCF (Scheme S1, ESI†).

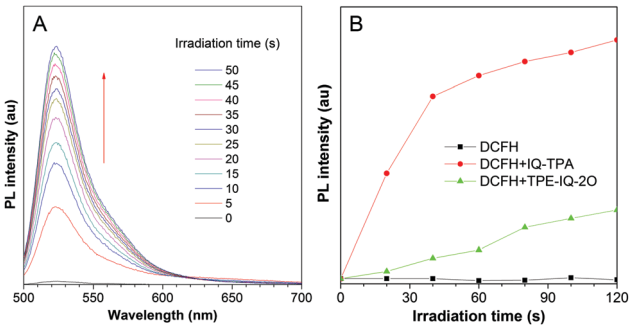

Fig. 2 (A) PL spectra of mixtures of IQ-TPA and DCFH in PBS (1% DMSO) under white light irradiation for different times. (B) Change in fluorescence intensity at 525 nm of AIEgens and DCFH in PBS upon white light irradiation for different times. Concentration: 5 μM for AIEgens and 1 μM for DCFH. Excitation: 488 nm.

As shown in Fig. 2A, with the mixture of IQ-TPA and DCFH under white light irradiation, the green fluorescence of DCF at 523 nm increased with increasing irradiation time. Compared to TPE-IQ-2O, IQ-TPA exhibits a much higher ROS generation rate (a steeper slope), suggesting IQ-TPA is a promising PS. The high ROS generation rate of IQ-TPA should be attributed to the longer absorption wavelength of the extended D–π–A conjugation and also the accompanying smaller singlet–triplet energy gap, which is reported to be beneficial for the enhancement of the ISC process.[27] In consideration of the complexity of the biological system, we further carried out experiments to confirm the ROS photosensitized by IQ-TPA in living cells by using DCFH-DA, a DCFH diacetate used for ROS detection in live cells (Fig. S1, ESI†). The fluorescence intensity at 525 nm from the HeLa cells co-stained with IQ-TPA and DCFH-DA increased with both the prolongation of light irradiation time and the dye pre-incubation time, suggesting the effectiveness of ROS generation sensitized by IQ-TPA in live cells.

Mitochondrial targeting cell imaging

The cationic structure of the isoquinolinium core is believed to serve as the mitochondrial targeting group of TPE-IQ and TPE-IQ-2O driven by the negative potential of the mitochondrial membrane.[13a] To verify the mitochondrial targeting ability of IQ-TPA, HeLa cells were co-stained with IQ-TPA and MitoTracker Red FM (MTR), which has much longer excitation and emission wavelengths than IQ-TPA to avoid signal overlap. As shown in Fig. 3A–D, the yellow fluorescence from IQ-TPA and the red fluorescence from MTR overlapped perfectly, suggesting the specific mitochondrial targeting of IQ-TPA. Moreover, as an important requirement for imaging and tracking, the photostability of IQ-TPA was tested. As shown in Fig. 3E, after 40 scans, there was almost no signal loss for IQ-TPA, while under the same laser power (0.10 μW), commercial MitoTracker Green FM shows a 70% signal loss. This result suggests IQ-TPA has a high photostability and is suitable for mitochondrial change monitoring.

One-photon excited PDT

Since fluorescent bioprobes based on traditional fluorophores suffer from the ACQ effect, they are often used at dilute concentrations resulting in low sensitivity and poor photostability.[7a,12d] The enhanced fluorescence and good photostability of the AIE PS IQ-TPA enables us to real-time monitor the mitochondrial change in cancer cells, which is important to determine the light dose and evaluate the therapeutic effect during the PDT process. As shown in Fig. 4A–C, during the light irradiation, the long tubular-like mitochondria gradually changed into disconnected and swollen vesicles, implying the mitochondria are damaged by ROS, which may consequently trigger the cell apoptotic pathway.[15b,28]

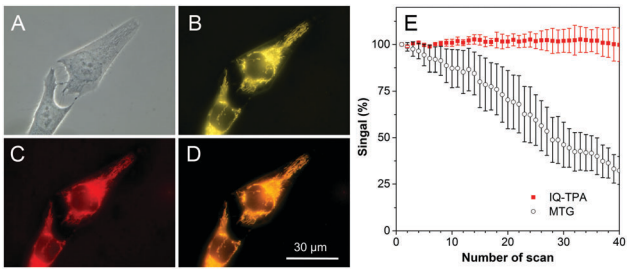

Fig. 3 Colocalization with commercial mitochondrial targeting dye MitoTracker Red FM (MTR). (A) Bright field and (B and C) fluorescent image of HeLa cells co-stained with (B) 200 nM of IQ-TPA and (C) 200 nM of MTR for 10 min. (D) Merged image of (B) and (C). Excitation: 400–440 nm for IQ-TPA and 540–580 nm for MTR. Scale bar: 30 μm. (E) Photostability of IQ-TPA by recording signal intensity retained after continuous scans. HeLa cells were stained with 200 nM IQ-TPA or MitoTracker Green FM for 20 min. Scanning time: 15.5 s per scan. Excitation: 405 nm for IQ-TPA and 488 nm for MTG with the same laser power of 0.10 μW.

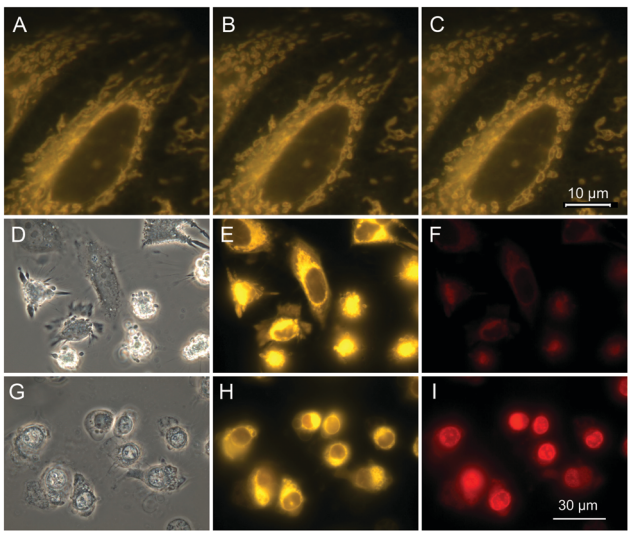

Fig. 4 (A–C) Monitoring the mitochondrial change during PDT by a fluorescence microscope. HeLa cells were incubated with IQ-TPA (1 μM) for 30 min and exposed to light irradiation with different durations: (A) 1 s, (B) 10 s and (C) 20 s. (D–I) Assessment of cell viability of the HeLa cells by propidium iodide (PI) after post-incubation for (D–F) 3 h and (G–I) 18 h. (D and G) Bright field images and (E and H) fluorescence images of IQ-TPA, (F and I) fluorescence images of PI. HeLa cells were incubated with IQ-TPA (1 μM) for 30 min and exposed to light irradiation for 15 min and further incubated in the dark for 3 h and 18 h. Before imaging, the HeLa cells were incubated with 1.5 μM of PI for 15 min. Excitation: 460–490 nm for IQ-TPA and 510–550 nm for PI.

To confirm IQ-TPA can induce cell apoptosis with PDT, the HeLa cells were further stained with propidium iodide (PI) after light irradiation of the IQ-TPA-stained cells. PI is not cell-permeable to live cells with an intact plasma membrane and can stain the nucleus of late apoptotic and necrotic cells with bright red fluorescence.[12d] As shown in Fig. 4D–F, 3 h after the PDT treatment, the cells shrank and even fragmented into multiple spherical vesicles, exhibiting the typical morphology of apoptotic cells.[1d] However, the nucleus of these cells still could not be stained by PI, suggesting the plasma membranes of these cells remained intact and the cells were at the early stage of apoptosis. With the prolongation of the post-incubation time, as shown in Fig. 4G–I, most of the cells treated with PDT exhibited red fluorescence in the nuclear regions. Such results can be also seen in a larger field of view (Fig. S2 and S3, ESI†). Meanwhile, the cells treated with IQ-TPA or light irradiation alone enjoyed a good survival rate (Fig. S3, ESI†), demonstrating that IQ-TPA possesses low dark cytotoxicity and can serve as a biocompatible PDT agent for cancer cell ablation. Compared to necrosis, cell apoptosis during the PDT treatment is beneficial for practical applications because apoptotic cells would be cleared by immune systems *in vivo* and thus greatly reduce the occurrence of inflammation.[1d] The apoptotic pathway should be attributed to the mitochondrial targeting of IQ-TPA as the sensitized ROS only damages the mitochondrial membranes rather than the plasma membrane during PDT and the consequent mitochondrial dysfunction induces cell apoptosis.[16d]

Furthermore, the PDT effect of IQ-TPA was evaluated by MTT assay. As shown in Fig. S4 (ESI†), the PDT effect of IQ-TPA can be elevated by the increase of dye concentration, dye pre-incubation time, light irradiation time and light intensity. It is noted that increasing the dye concentration would lead to a slight dark cytotoxicity to cells. This could be explained by the increased accumulation of IQ-TPA in the mitochondrial region leading to the depolarization of the MMP causing cell death.[12c] However, with a moderate dark cytotoxicity, the dye concentration of 1 μM was chosen for optimizing other factors. Under the condition that HeLa cells were pre-incubated with 1 μM IQ-TPA for 30 min and then subjected to white light irradiation for 15 min with a light density of 60 mW cm^{-2}, a cell viability of $<20\%$ was achieved. Compared to previous PS systems,[16b,17,18] the low dose, short dye incubation time, short light irradiation time and moderate light intensity of IQ-TPA demonstrates the facile, material-saving and time-saving approach of PDT.

Two-photon excited PDT

With one-photon visible excitation, we have demonstrated mitochondrial targeting IQ-TPA with a high ROS generation rate can effectively kill cancer cells. Thus, it is expected that its large δ_{TPA} would enable IQ-TPA to effectively kill cancer cells through two-photon NIR excitation. To demonstrate the feasibility, two-photon imaging and TP-PDT were then studied under a two-photon microscope with a femtosecond Ti:sapphire laser. As shown in Fig. 5, regardless of the higher brightness of IQ-TPA with one-photon excitation (~5 folds), a much stronger two-photon excited fluorescence (~15 folds) was observed for IQ-TPA

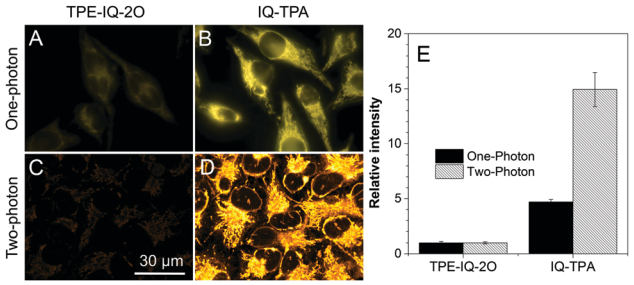

Fig. 5 (A and B) One-photon and (C and D) two-photon excited fluorescence images of HeLa cells stained with 500 nM (A and C) TPE-IQ-2O or (B and D) IQ-TPA for 30 min. (E) Relative fluorescence intensity of IQ-TPA compared to TPE-IQ-2O with one/two-photon imaging. Excitation: 400–440 nm for one-photon imaging by a fluorescence microscope and 900 nm (3 mW) for two-photon imaging by a two-photon microscope. The error bar was obtained by the intensity data of five regions of interest in each image.

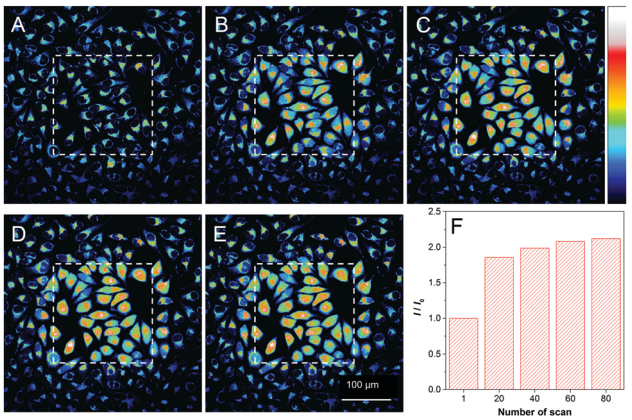

Fig. 6 Detection of intracellular ROS generation in HeLa cells using DCFH-DA. (A–F) The fluorescence images of DCF (excitation: 488 nm, emission: 500–530 nm) are shown and the intensity was encoded with Royal colour. HeLa cells were incubated with IQ-TPA (1 μM) and DCFH-DA (10 μM) for 30 min followed by different two-photon scans: (A) 1 scan, (B) 20 scans, (C) 40 scans, (D) 60 scans and (E) 80 scans. The scanned area of 200 × 200 μm^2 is shown by white squares. The two-photon excitation condition was at 900 nm (fs Ti:sapphire laser, 8 mW) with a scan speed of 10.28 s per scan. (F) Plot of averaged intensity within the white squares *versus* the number of two-photon scans.

than that of TPE-IQ-2O, suggesting IQ-TPA is promising for two-photon imaging. Similar to the one-photon excited PDT, the intracellular ROS generation increased with increasing two-photon excitation time (Fig. 6). Then, the mitochondrial changes of HeLa cells stained with IQ-TPA were monitored by two-photon excitation (900 nm). As shown in Fig. 7, with increasing two-photon scans, the reticulum-like mitochondrial structures were gradually fragmented and granulated after 100 scans, once again demonstrating the good photostability and PDT effect of IQ-TPA.

To analyze the efficiency of IQ-TPA in TP-PDT action, HeLa cells were first incubated with IQ-TPA for 30 min, followed by a series of two-photon scans. After post-incubation for 18 h, the cells were stained with fluorescein diacetates (FDA) and PI for

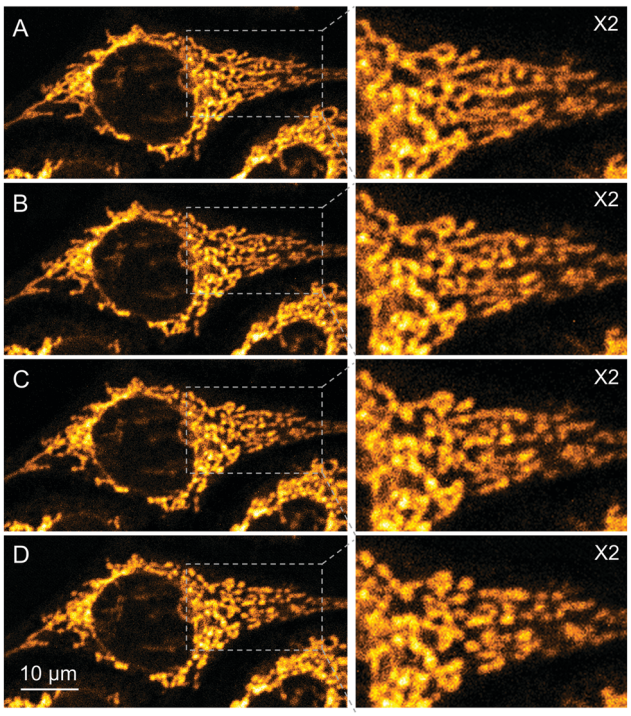

Fig. 7 Monitoring the mitochondrial change during TP-PDT by the fluorescence of IQ-TPA. Fluorescence images of HeLa cells were incubated with 1 μM of IQ-TPA for 30 min and then followed by two-photon scans: (A) 1 scan, (B) 33 scans, (C) 66 scans and (D) 100 scans. The two-photon excitation condition was at 900 nm (fs Ti:sapphire laser, 5 mW) with a scan area of 60 × 60 μm^2 and a scan speed of 1.02 s per scan.

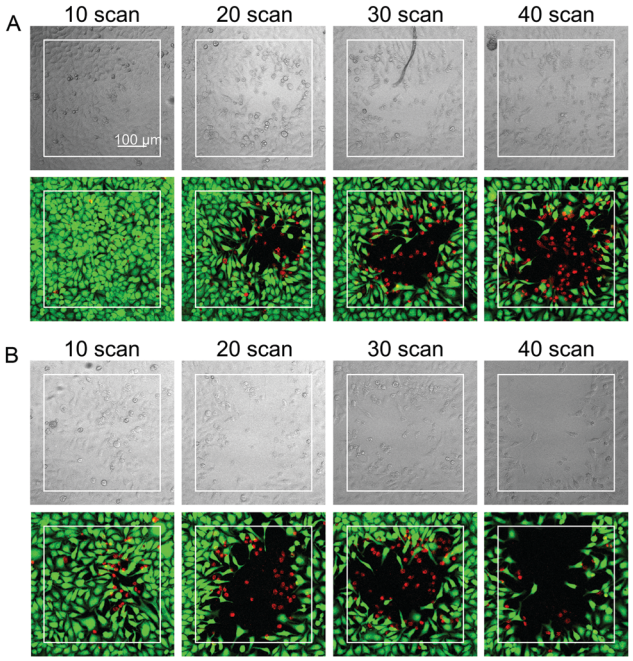

Fig. 8 Cell viability of HeLa cells treated with TP-PDT of IQ-TPA assessed by fluorescein diacetates (FDA) and propidium iodide (PI). Bright field and fluorescent overlay images of HeLa cells are shown. HeLa cells were incubated with IQ-TPA (1 μM, 30 min) followed by different two-photon scans at the laser power of (A) 8 mW and (B) 11 mW. After 18 h post-incubation, the cells were stained with FDA and PI to assess cell viability. The two-photon excitation condition was at 900 nm (fs Ti:sapphire laser) with a scan speed of 10.28 s per scan. The scanned areas of 387.5 × 387.5 μm^2 are shown by white squares. Excitation/emission: 488/500–530 nm for FDA and 561/600–650 nm for PI.

15 min for cell viability evaluation. In contrast to PI, FDA is a cell-permeant esterase substrate and can serve as a probe for live cells with strong green fluorescence. As shown in Fig. 8, almost all the cells outside the scanned areas showed FDA fluorescence, indicating the good biocompatibility of IQ-TPA. In the scanned areas, when the number of scans was 10, very few cells are PI-positive. With the increase of scans, more cells become PI-positive. The scan number required to kill 50% the cells (LD_{50}) was used to estimate the TP-PDT efficiency and studied under different laser powers (Fig. 8, Fig. S5 and S6, ESI†). When the laser power is 20 mW, only 14 scans are enough to kill 50% of the cells, but at 8 mW, 45 scans are required to achieve a similar effect. Despite a much larger scanned area, the light dose was calculated to be 3700 J cm^{-2} (8 mW, 387.5 × 387.5 μm^2), which is comparable to that of 2720 J cm^{-2} (6.8 mW, 230 × 230 μm^2) using porphyrin derivatives with ultrahigh δ_{TPA} and that of 4500 J cm^{-2} (7.5 mW, 243 × 243 μm^2) using polymer-encapsulated AIE organic dots.[16b,17] Meanwhile, no signs of cytotoxicity in HeLa cells were found for the NIR laser irradiation alone with a light dose of up to 7200 J cm^{-2} in our experimental results (Fig. S7, ESI†) and that of others,[17] further proving the efficacy of TP-PDT of IQ-TPA in killing cancer cells. Compared to one-photon PDT, TP-PDT has the superior advantages of a higher penetration depth by NIR light and high 3D resolution for the elimination of damage to healthy cells in the light beam, which is highly desirable for *in vivo* diagnosis and the delicate therapeutic treatment of cancer. Compared to the FRET-based TP-PDT systems with complicated synthesis and multiple components,[15c,19b,c,29] this example of utilizing the simple small-molecule AIEgen with multifunctionalities for TP-PDT shows the great feasibility of the one-for-all approach for future theranostics.

Conclusions

To conclude, in this work, we reported a simple AIE luminogen, IQ-TPA, with mitochondrial targeting and susceptible two-photon excitation for image-guided TP-PDT in cancer cells. The mitochondrial targeting IQ-TPA enables efficient ROS generation in the mitochondrial region under both white light irradiation and two-photon excitation at 900 nm, causing damage to mitochondria and finally leading to mitochondria-mediated cell apoptosis with the merits of low dose, short incubation time and irradiation time. IQ-TPA also exhibits high brightness and good photostability and is suitable for localizing dyes, monitoring cellular damage and evaluating the therapeutic effect during PDT. More importantly, we successfully utilized IQ-TPA to kill cancer cells *via* TP-PDT, showing its great potential for precise cancer treatment and the great feasibility of the one-for-all approach for future theranostics.

Conflicts of interest

There are no conflicts to declare.

Acknowledgements

This work was partially supported by the Innovation and Technology Commission (ITC-CNERC14SC01), the National Basic Research Program of China (973 Program: 2013CB834701 and 2013CB834702), the University Grants Committee of Hong Kong (AoE/P-03/08) and the Research Grants Council of Hong Kong (16301614, 16305015, N_HKUST604/14 and A-HKUST605/16). B. Z. T. is also grateful for the support from the Guangdong Innovative Research Team Program of China (201101C0105067115), and the Science and Technology Plan of Shenzhen (JCYJ20160229205601482).

Notes and references

1 (*a*) R. R. Allison, G. H. Downie, R. Cuenca, X.-H. Hu, C. J. H. Childs and C. H. Sibata, *Photodiagn. Photodyn. Ther.*, 2004, **1**, 27–42; (*b*) R. R. Allison and C. H. Sibata, *Photodiagn. Photodyn. Ther.*, 2010, **7**, 61–75; (*c*) A. P. Castano, T. N. Demidova and M. R. Hamblin, *Photodiagn. Photodyn. Ther.*, 2004, **1**, 279–293; (*d*) A. P. Castano, T. N. Demidova and M. R. Hamblin, *Photodiagn. Photodyn. Ther.*, 2005, **2**, 1–23; (*e*) A. P. Castano, T. N. Demidova and M. R. Hamblin, *Photodiagn. Photodyn. Ther.*, 2005, **2**, 91–106.

2 (*a*) M. Wainwright, *Photodiagn. Photodyn. Ther.*, 2005, **2**, 263–272; (*b*) E. S. Nyman and P. H. Hynninen, *J. Photochem. Photobiol., B*, 2004, **73**, 1–28.

3 (*a*) W. Z. Yuan, P. Lu, S. Chen, J. W. Y. Lam, Z. Wang, Y. Liu, H. S. Kwok, Y. Ma and B. Z. Tang, *Adv. Mater.*, 2010, **22**, 2159–2163; (*b*) B. Chen, G. Feng, B. He, C. Goh, S. Xu, G. Ramos-Ortiz, L. Aparicio-Ixta, J. Zhou, L. Ng, Z. Zhao, B. Liu and B. Z. Tang, *Small*, 2016, **12**, 782–792.

4 J. Mei, N. L. C. Leung, R. T. K. Kwok, J. W. Y. Lam and B. Z. Tang, *Chem. Rev.*, 2015, **115**, 11718–11940.

5 Y. Zhang, D. Li, Y. Li and J. Yu, *Chem. Sci.*, 2014, **5**, 2710–2716.

6 H. Shi, R. T. K. Kwok, J. Liu, B. Xing, B. Z. Tang and B. Liu, *J. Am. Chem. Soc.*, 2012, **134**, 17972–17981.

7 (*a*) C. W. T. Leung, Y. Hong, S. Chen, E. Zhao, J. W. Y. Lam and B. Z. Tang, *J. Am. Chem. Soc.*, 2013, **135**, 62–65; (*b*) M. Gao, C. K. Sim, C. W. T. Leung, Q. Hu, G. Feng, F. Xu, B. Z. Tang and B. Liu, *Chem. Commun.*, 2014, **50**, 8312–8315.

8 D. Ding, D. Mao, K. Li, X. Wang, W. Qin, R. Liu, D. S. Chiam, N. Tomczak, Z. Yang, B. Z. Tang, D. Kong and B. Liu, *ACS Nano*, 2014, **8**, 12620–12631.

9 W. Qin, D. Ding, J. Liu, W. Z. Yuan, Y. Hu, B. Liu and B. Z. Tang, *Adv. Funct. Mater.*, 2012, **22**, 771–779.

10 (*a*) D. Ding, K. Li, B. Liu and B. Z. Tang, *Acc. Chem. Res.*, 2013, **46**, 2441–2453; (*b*) X. Zhang, K. Wang, M. Liu, X. Zhang, L. Tao, Y. Chen and Y. Wei, *Nanoscale*, 2015, **7**, 11486–11508.

11 (*a*) Y. Yuan, G. Feng, W. Qin, B. Z. Tang and B. Liu, *Chem. Commun.*, 2014, **50**, 8757–8760; (*b*) M. Gao, Q. Hu, G. Feng, N. Tomczak, R. Liu, B. Xing, B. Z. Tang and B. Liu, *Adv. Healthcare Mater.*, 2015, **4**, 659–663; (*c*) Y. Yuan, C.-J. Zhang, M. Gao, R. Zhang, B. Z. Tang and B. Liu, *Angew. Chem., Int. Ed.*, 2015, **54**, 1780–1786; (*d*) G. Jin, G. Feng, W. Qin, B. Z. Tang, B. Liu and K. Li, *Chem. Commun.*, 2016, **52**, 2752–2755; (*e*) G. Feng, W. Wu, S. Xu and B. Liu, *ACS Appl. Mater. Interfaces*, 2016, **8**, 21193–21200; (*f*) G. Feng, Y. Fang, J. Liu, J. Geng, D. Ding and B. Liu, *Small*, 2017, **13**, 1602807.

12 (*a*) V. Gogvadze, S. Orrenius and B. Zhivotovsky, *Semin. Cancer Biol.*, 2009, **19**, 57–66; (*b*) W. S. Shin, M.-G. Lee, P. Verwilst, J. H. Lee, S.-G. Chi and J. S. Kim, *Chem. Sci.*, 2016, **7**, 6050–6059; (*c*) C.-J. Zhang, Q. Hu, G. Feng, R. Zhang, Y. Yuan, X. Lu and B. Liu, *Chem. Sci.*, 2015, **6**, 4580–4586; (*d*) E. Zhao, H. Deng, S. Chen, Y. Hong, C. W. T. Leung, J. W. Y. Lam and B. Z. Tang, *Chem. Commun.*, 2014, **50**, 14451–14454.

13 (*a*) C. Gui, E. G. Zhao, R. T. K. Kwok, A. C. S. Leung, J. W. Y. Lam, M. J. Jiang, H. Q. Deng, Y. J. Cai, W. J. Zhang, H. F. Su and B. Z. Tang, *Chem. Sci.*, 2017, **8**, 1822–1830; (*b*) C. Y. Y. Yu, H. Xu, S. Ji, R. T. K. Kwok, J. W. Y. Lam, X. Li, S. Krishnan, D. Ding and B. Z. Tang, *Adv. Mater.*, 2017, **29**, 1606167.

14 (*a*) A. R. Oseroff, D. Ohuoha, G. Ara, D. McAuliffe, J. Foley and L. Cincotta, *Proc. Natl. Acad. Sci. U. S. A.*, 1986, **83**, 9729–9733; (*b*) J. S. Modica-Napolitano and J. R. Aprille, *Adv. Drug Delivery Rev.*, 2001, **49**, 63–70.

15 (*a*) Y.-Y. Huang, P. Mroz, T. Zhiyentayev, S. K. Sharma, T. Balasubramanian, C. Ruzié, M. Krayer, D. Fan, K. E. Borbas, E. Yang, H. L. Kee, C. Kirmaier, J. R. Diers, D. F. Bocian, D. Holten, J. S. Lindsey and M. R. Hamblin, *J. Med. Chem.*, 2010, **53**, 4018–4027; (*b*) W. Hu, T. He, R. Jiang, J. Yin, L. Li, X. Lu, H. Zhao, L. Zhang, L. Huang, H. Sun, W. Huang and Q. Fan, *Chem. Commun.*, 2017, **53**, 1680–1683; (*c*) J. R. Starkey, A. K. Rebane, M. A. Drobizhev, F. Meng, A. Gong, A. Elliott, K. McInnerney and C. W. Spangler, *Clin. Cancer Res.*, 2008, **14**, 6564–6573.

16 (*a*) J. Bhawalkar, N. Kumar, C.-F. Zhao and P. Prasad, *J. Clin. Laser Med. Surg.*, 1997, **15**, 201–204; (*b*) H. A. Collins, M. Khurana, E. H. Moriyama, A. Mariampillai, E. Dahlstedt, M. Balaz, M. K. Kuimova, M. Drobizhev, V. X. D. Yang, D. Phillips, A. Rebane, B. C. Wilson and H. L. Anderson, *Nat. Photonics*, 2008, **2**, 420–424; (*c*) Q. Zou, Y. Fang, Y. Zhao, H. Zhao, Y. Wang, Y. Gu and F. Wu, *J. Med. Chem.*, 2013, **56**, 5288–5294; (*d*) R. Chennoufi, H. Bougherara, N. Gagey-Eilstein, B. Dumat, E. Henry, F. Subra, S. Bury-Mone, F. Mahuteau-Betzer, P. Tauc, M. P. Teulade-Fichou and E. Deprez, *Sci. Rep.*, 2016, **6**, 21458.

17 B. Gu, W. Wu, G. Xu, G. Feng, F. Yin, P. H. J. Chong, J. Qu, K.-T. Yong and B. Liu, *Adv. Mater.*, 2017, **29**, 1701076.

18 M. Khurana, H. A. Collins, A. Karotki, H. L. Anderson, D. T. Cramb and B. C. Wilson, *Photochem. Photobiol.*, 2007, **83**, 1441–1448.

19 (*a*) S. Kim, T. Y. Ohulchanskyy, H. E. Pudavar, R. K. Pandey and P. N. Prasad, *J. Am. Chem. Soc.*, 2007, **129**, 2669–2675; (*b*) Y. Shen, A. J. Shuhendler, D. Ye, J.-J. Xu and H.-Y. Chen, *Chem. Soc. Rev.*, 2016, **45**, 6725–6741; (*c*) M. A. Oar, W. R. Dichtel, J. M. Serin, J. M. J. Fréchet, J. E. Rogers, J. E. Slagle, P. A. Fleitz, L.-S. Tan, T. Y. Ohulchanskyy and P. N. Prasad, *Chem. Mater.*, 2006, **18**, 3682–3692.

20 G. Feng and B. Liu, *Small*, 2016, **12**, 6528–6535.
21 M. Jiang, X. Gu, R. T. K. Kwok, Y. Li, H. H. Y. Sung, X. Zheng, Y. Zhang, J. W. Y. Lam, I. D. Williams, X. Huang, K. S. Wong and B. Z. Tang, *Adv. Funct. Mater.*, 2017, DOI: 10.1002/adfm.201704589.
22 (*a*) C. Allain, F. Schmidt, R. Lartia, G. Bordeau, C. Fiorini-Debuisschert, F. Charra, P. Tauc and M.-P. Teulade-Fichou, *ChemBioChem*, 2007, **8**, 424–433; (*b*) R. Lartia, C. Allain, G. Bordeau, F. Schmidt, C. Fiorini-Debuisschert, F. Charra and M.-P. Teulade-Fichou, *J. Org. Chem.*, 2008, **73**, 1732–1744; (*c*) Y. Liu, M. Kong, Q. Zhang, Z. Zhang, H. Zhou, S. Zhang, S. Li, J. Wu and Y. Tian, *J. Mater. Chem. B*, 2014, **2**, 5430–5440.
23 M. Pawlicki, H. A. Collins, R. G. Denning and H. L. Anderson, *Angew. Chem., Int. Ed.*, 2009, **48**, 3244–3266.
24 J. Jayakumar, K. Parthasarathy and C.-H. Cheng, *Angew. Chem., Int. Ed.*, 2012, **51**, 197–200.
25 D. H. Oh, B. A. King, S. G. Boxer and P. C. Hanawalt, *Proc. Natl. Acad. Sci. U. S. A.*, 2001, **98**, 11271–11276.
26 M. Albota, D. Beljonne, J.-L. Brédas, J. E. Ehrlich, J.-Y. Fu, A. A. Heikal, S. E. Hess, T. Kogej, M. D. Levin, S. R. Marder, D. McCord-Maughon, J. W. Perry, H. Röckel, M. Rumi, G. Subramaniam, W. W. Webb, X.-L. Wu and C. Xu, *Science*, 1998, **281**, 1653–1656.
27 (*a*) J. Li, Y. Jiang, J. Cheng, Y. Zhang, H. Su, J. W. Y. Lam, H. H. Y. Sung, K. S. Wong, H. S. Kwok and B. Z. Tang, *Phys. Chem. Chem. Phys.*, 2015, **17**, 1134–1141; (*b*) S. Xu, Y. Yuan, X. Cai, C.-J. Zhang, F. Hu, J. Liang, G. Zhang, D. Zhang and B. Liu, *Chem. Sci.*, 2015, **6**, 5824–5830.
28 D.-F. Suen, K. L. Norris and R. J. Youle, *Genes Dev.*, 2008, **22**, 1577–1590.
29 K. Ogawa, H. Hasegawa, Y. Inaba, Y. Kobuke, H. Inouye, Y. Kanemitsu, E. Kohno, T. Hirano, S.-I. Ogura and I. Okura, *J. Med. Chem.*, 2006, **49**, 2276–2283.